Mesoporous silica as topical nanocarriers for quercetin: characterization and in vitro studies

UNIVERSITÀ DEGLI STUDI DI TORINO

Mesoporous silica as topical nanocarriers for quercetin: characterization and *in vitro* studies

Simona Sapino[a,c,d], Elena Ugazio[a,c,d*], Lucia Gastaldi[a], Ivana Miletto[b,c], Gloria Berlier[b,c], Daniele Zonari[a], Simonetta Oliaro-Bosso[a,d]

[a]*Università di Torino, Dipartimento di Scienza e Tecnologia del Farmaco, Via Giuria 9, 10125 Torino, Italy.*

[b]*Università di Torino, Dipartimento di Chimica, Via Giuria 7, 10125 Torino, Italy.*

[c]*NIS (Nanostructured Interfaces and Surfaces) Centre, Università di Torino, Italy.*

[d] *"G. Scansetti" Interdepartmental Centre, Università di Torino, Italy.*

**Corresponding author: Tel: +39 0116707192; Fax: +39 0116707687*

E-mail address: elena.ugazio@unito.it

ABSTRACT

The flavonoid quercetin is extensively studied for its antioxidant and chemopreventive properties. However the poor water-solubility, low stability and short half-life could restrict its use in skin care products and therapy.

The present study is aimed to evaluate the potential of aminopropyl functionalized mesoporous silica nanoparticles (NH_2-MSN) as topical carrier system for quercetin delivery. Thermo gravimetric analysis, X-ray diffraction, high resolution transmission electron microscopy, nitrogen adsorption isotherms, FT-IR spectroscopy, zeta potential measurements and differential scanning calorimetry allowed analyzing with great detail the organic-inorganic molecular interaction.

The protective effect of this vehicle on UV-induced degradation of the flavonoid was investigated revealing a certain positive influence of the inclusion on the photostability over time.

Epidermal accumulation and transdermal permeation of this molecule were *ex vivo* evaluated using porcine skin mounted on Franz diffusion cells. The inclusion complexation with the inorganic nanoparticles increased the penetration of quercetin into the skin after 24 h post-application without transdermal delivery.

The effect of quercetin alone or given as complex with NH_2-MSN on proliferation of JR8 human melanoma cells was evaluated by sulforhodamine B colorimetric proliferation assay. At a concentration 60 μM the complex with NH_2-MSN was more effective than quercetin alone, causing about 50% inhibition of cell proliferation.

Keywords: NH_2-MCM-41 nanoparticles, quercetin delivery, photostability, cytotoxicity, skin uptake

1. Introduction

Flavonoids have recently attracted great interest because of their potential beneficial effects on human health: they are reported to have antiviral, anti-allergic, antiplatelet, anti-inflammatory, antitumor and antioxidant activities [1, 2]. Among flavonols, quercetin (3,5,7,3′,4′-pentahydroxyflavone) is recognized as a strong antioxidant because it can chelate metals, scavenge oxygen free radicals [3, 4] and *in vitro* inhibits xanthine oxidase and lipid peroxidation [5-7].

In addition, quercetin has been shown to be able to counteract UV-induced oxidative skin damage following topical application to the skin. These facts coupled with its safety and natural origin make this molecule an attractive candidate for incorporation into personal care formulations [8]. In cultured cells quercetin, depending on the conditions of exposure, shows either antioxidant or pro-oxidant effects [9]. Quercetin has also received greater attention as pro-apoptotic flavonoid with a specific and almost exclusive activity on tumor cell lines rather than normal, non-transformed cells [10].

Due to its antioxidant, antitumor and anti-inflammatory activity, quercetin has been studied extensively as a chemoprevention agent in several cancer models [11]. Several *in vitro* studies have shown consistent anticancer effects of quercetin in a variety of cancer cell lines and tumors, including U138MG (glioma) [12], HeLa (cervical cancer) [13], MDA-MB-453 (breast cancer) [14], HT-29 (colorectal xenografts) [15], myeloid leukemia [16] and oral cavity cancer [17].

As for the biochemical mechanism, recent studies have revealed that quercetin inhibits cell proliferation by causing apoptosis and/or cell cycle arrest [18, 19]. It has been shown that quercetin treatment causes cell cycle arrests such as G_2/M arrest or G_1 arrest in different cell types [20-22]. Moreover, quercetin-mediated apoptosis may result from the induction of stress proteins, disruption of microtubules and mitochondria, release of cytochrome *c*, and activation of caspases [23]. The ability of quercetin to interfere with different targets identified as hallmarks of cancer makes this molecule a multi-target inhibitor with pleiotropic and synergistic effects in tumor cells [11].

However its poor water solubility, low stability and short half-life have so far hampered its introduction in therapy and clinical practices.

To overcome these inconveniences the use of supramolecular structures as nanoparticles or microparticles was proposed. Specifically, quercetin was included in cyclodextrins [24], covalently conjugated into a polymethacrylic acid backbone [25] or entrapped in chitosan nanoparticles [26] and liposomes [27]. However, most of these strategies allow little control over the nanocarrier size and poor versatility.

Recently the use of ordered mesoporous materials as drug delivery systems (DDS), firstly reported by Vallet-Regí *et al*. [28], has become increasingly popular, as testified by the abundant literature on mesoporous silica nanoparticles (MSN) as DDS [29-32].

The extremely high surface area, ordered porosity and tunable pore volume of this bioactive oxide are ideal properties for high drug loading and diffusion-driven gradual release [33-35]. In addition, it is possible to chemically modify the surface properties through covalent grafting of various organic functional groups to the free silanol groups [36].

Nevertheless, few papers report the employment of MCM-41-type mesoporous silica as carrier system for the topical delivery of active agents [37-40].

Mesoporous silica is expected to have relatively good stability and biocompatibility, even if its fate in physiological fluids and the actual effect on cells is still the object of many studies, especially when nanoparticles are employed [31, 41-48].

Our previous studies on Trolox®, quercetin and rutin, indicate that mesoporous silica is an innovative carrier suitable for topical application of antioxidants [39, 49, 50].

In this study we report on the immobilization of quercetin in aminopropyl-functionalized MCM-41 mesoporous silica nanoparticles. The quercetin-loading capacity has been determined either spectrophotometrically or by thermo gravimetric analysis (TGA). A particular attention has been devoted to the physico-chemical properties of the inclusion complex. Therefore several analytic techniques (XRD, HRTEM, N_2 adsorption analysis, FT-IR spectroscopy, zeta potential

measurements and DSC) have been employed to characterize the nanoparticles before and after complexation. The quercetin diffusion through a cellulose membrane has been studied, and the photostability of the included molecule has been analyzed upon UV irradiation. With a view to a possible use of quercetin in topical formulations, based on its antioxidant and protective properties, an *ex vivo* study using Franz diffusion cells was performed to investigate the influence of the inclusion in silica nanoparticles on the skin uptake of quercetin. Moreover *in vitro* cytotoxicity on JR8 human melanoma cells was tested in order to evaluate the chemoprevention potential of this innovative nanosized complex, compared to that of free quercetin.

2. Materials and methods

2.1. Materials

3,3',4',5,7-Pentahydroxyflavone dihydrate (Quercetin dihydrate, Q) n-cetyl-trimethylammonium bromide (CTAB), tetraethyl orthosilicate (TEOS), 3-aminopropyl triethoxysilane (APTES), isopropyl myristate, toluene, magnesium sulfate, sodium chloride, sodium azide, sulforhodamine B (SRB), RPMI-1640 medium, fetal calf serum, Tris buffered saline, trichloroacetic acid and antibiotics for cell cultures were purchased from Sigma-Aldrich (Milan, Italy). Methanol, absolute ethanol, acetic acid and sodium acetate were from Fluka (Milan, Italy). Potassium palmitoyl hydrolyzed wheat protein and glyceryl stearate and cetearyl alcohol (Phytocream® 2000) was from Sinerga (Pero, Milan, Italy). Cetearyl isononanoate (Tegosoft® CI), caprylic/capric triglycerides (Tegosoft® CT), dimethicone (Abil® 350) and glycerol were ACEF (Fiorenzuola D'Arda, Piacenza, Italy) products. Carbomer (Carbopol® ETD 2001) was from Noveon (Brussels, Belgium), and PEG-30 dipolyhydroxystearate (Arlacel® P135) from Croda (Mortara, Pavia, Italy).

JR8 human melanoma cells were kindly provided by Dr. Chiara Dianzani (University of Torino, Dipartimento di Scienza e Tecnologia del Farmaco, Torino, Italy).

2.2. Synthesis of MCM-41 nanoparticles

Purely siliceous MCM-41 nanoparticles (MSN) were synthesized by optimizing a literature procedure, employing CTAB as the Structure Directing Agent (SDA) and TEOS as the silica source [51, 52]. SDA was removed by calcination at 550 °C, first under nitrogen and subsequently under oxygen flow. Aminopropyl-functionalized MCM-41 nanoparticles (NH_2-MSN) were prepared by suspending 1.0 g of calcined MSN in 30 mL of toluene. Next, 0.6 mL of APTES were added drop-wise and the mixture was allowed to reflux for 8 h. The reaction solution was centrifuged and the deposited gel washed first with ethanol and then with deionized water. The obtained white solid was filtered, washed with methanol and dried *in vacuum*.

2.3. Quercetin loading

Q inclusion complexes were prepared by impregnation method in 1/3, 1/1, 3/1 w/w ratio. Different aliquots (213.1 mg, 71.0 mg, 23.7 mg, respectively) of NH_2-MSN, previously outgassed at 150 °C for 1 h to remove the adsorbed water, were added to 10.0 mL of saturated Q methanol solution (21 mM). The mixtures were kept under magnetic stirring at room temperature (RT) for 24 h and, after centrifugation, each precipitate was dried under *vacuum*. As reference model, Q complex with non-functionalized nanoparticles was also prepared by the same method in 1/1 w/w ratio. The resulting complexes are hereafter labeled as Q/MSN and Q/NH_2-MSN.

2.4. Quercetin analysis

UV-Vis spectrophotometry calibration curves were obtained in different media with diluted Q solutions over the range 1.5-15.2×10^{-5} M. The molar extinction coefficient (ε) was 20432 M^{-1} (R^2 = 0.9985) in ethanol, 23551 M^{-1} (R^2 = 0.9998) in methanol and 17416 M^{-1} (R^2 = 0.9503) in ethanol/acetate buffer pH 5.0 (20/80).

HPLC analysis was performed employing an apparatus (Shimadzu) consisting of a LC-6A pump unit control, a SPD-2A UV-Vis detector, a C-R3A chromatopac integrator and a RP-C18 column

(Waters, 150×4.6 mm; 5 µm). Q was eluted with a mixture of methanol/water/acetic acid (50/47/3 v/v/v) and its flow rate was kept at 0.8 mL/min. The elution profile was monitored at 371 nm and the retention time of Q was about 4.5 min. The amount of Q in the samples was quantified, based on the standard curve generated by calculating HPLC peak area of pure Q (in ethanol ε was 2.50×10^{10} M^{-1} (R^2 = 0.9961), while in ethanol/acetate buffer pH 5.0 (80/20) was 5.35×10^{10} M^{-1} (R^2 = 0.9994).

2.5. Physico-chemical characterization

2.5.1. Thermo gravimetric analysis

A thermo gravimetric analysis (TGA) was carried out on a TAQ600 (TA Instruments) heating the samples at a rate of 10 °C min^{-1} from 30 to 1000 °C in a nitrogen flow. Before starting the measurements, samples were equilibrated at 30 °C. Once reached the final temperature an isotherm was run for 15 min in air, to burn carbonaceous residues from pyrolysis reactions.

2.5.2. X-ray diffraction

Powder X-ray diffraction (XRD) patterns were collected on a X'Pert Pro Bragg Brentano diffractometer (Philips) using Cu Kα radiation (40 mA and 45 kV), with a scan speed of 0.01° min^{-1}.

2.5.3. High Resolution Transmission Electron Microscopy

High resolution transmission electron microscopy (HRTEM) observations were performed on a JEOL 3010 instrument operating at 300 kV. For the measurements, the powder was dispersed on a copper grid coated with a perforated carbon film.

2.5.4. N_2 adsorption analysis

Specific surface area (SSA), pore volume and size were measured by N_2 adsorption–desorption isotherms at -196 °C using ASAP 2020 gas-volumetric analyzer (Micromeritics). SSA was

calculated using the Brunauer-Emmet-Teller (BET) method, average pore size and volume were calculated on the adsorption branch of the isotherms according to the Barrett-Joyner-Halenda (BJH) method (Kruk-Jaroniec-Sayari equations). Prior to analyses, samples were outgassed at RT overnight.

2.5.5. FT-IR spectroscopy

Fourier transform infrared spectra (FT-IR) were recorded with Bruker IFS28 equipped with a MCT detector, working with resolution of 4 cm^{-1} over 64 scans. Samples were in the form of self-supporting pellets suitable for transmission infrared experiments and were placed in a quartz cell equipped with KBr windows, designed for RT studies *in vacuum* and controlled atmosphere. Before FT-IR analysis the samples were outgassed at RT to remove physically adsorbed water and impurities.

2.5.6. Zeta potential measurements

Zeta potential measurements of MSN, NH_2-MSN, Q/MSN_1/1 and Q/NH_2-MSN_1/1 were performed by means of electrophoretic light scattering (ELS) (Zetasizer Nano-ZS, Malvern Instruments). Each system was suspended in ultra-filtered water (0.1 % w/v), sonicated for about 10 min and then analyzed at 25 ± 0.1 °C. Zeta potential values were measured without altering the pH of the dispersion medium (7.0) and using the Smoluchowski equation; results are expressed as the mean ± S.D. of three runs.

2.5.7. Differential scanning calorimetry

Differential scanning calorimetry (DSC) analyses were performed on a DSC-7 power compensation thermal analyzer (Perkin Elmer), performing temperature calibration with indium as standard. 1-12 mg of samples having the same amount of Q were loaded in aluminum pans and heated under nitrogen flow at a scanning speed of 10 °C min^{-1} from 100 to 350 °C.

2.6. Testing of complex properties

2.6.1. Preparation of the emulsions

The O/W emulsion was made by adding, under homogenization by IKA T25 Ultra-Turrax, the melted lipid phase composed of Phytocream® 2000, Tegosoft® CI and Abil® 350 to a suspension of Carbopol® ETD 2001 and glycerol in ultrapure water, previously heated at 80 °C. The obtained system cooled to RT was then added with either Q or the complex Q/NH_2-MSN, previously dispersed in a small volume of ultrapure water. Finally, the pH was adjusted to 5.0 (Table S1).

To prepare the W/O emulsion the ultrapure water was heated at about 80 °C and then added with glycerol and magnesium sulfate. Meanwhile, the lipid phase consisting of Arlacel® P135, Tegosoft® CT and isopropyl myristate was weighed and melted on the hotplate without exceeding 60 °C. The aqueous phase was then slowly joined to the lipids homogenizing to obtain a homogeneous system. The emulsion was left to cool under slow mechanical stirring by paddle stirrer until it reached RT. For the addition of Q, either as such or complexed with NH_2-MSN, the same procedure described for the O/W emulsion was followed. The pH was adjusted to 5.0 (Table S2).

2.6.2. Quercetin transmembrane diffusion

The diffusion of Q through a Servapor® (12,000-14,000 MWCO, Serva Electrophoresis) cellulose dialysis membrane was investigated using a glass apparatus consisting of two horizontal cells each of 12 mL volume; the diffusion area was 2.92 cm^2. As donor phase, Q, free or complexed with NH_2-MSN, was dispersed in ethanol/acetate buffer mixture (20/80 v/v, pH 5.0) or in O/W emulsion to get 0.0034% w/w in the first and 0.0084% w/w in the latter system. The receiving phase was ethanol/acetate buffer (20/80 v/v, pH 5.0). At fixed times up to 24 h, an aliquot (0.3 mL) of the receiving phase was withdrawn, replaced with an equal volume of fresh medium, suitably diluted

and analyzed using the HPLC method previously described. The experiment was carried out in triplicate.

2.6.3. Photodegradation study

Irradiation tests were performed separately on pure Q and on Q/NH_2-MSN_1/1 complex. The runs were carried out in the ethanol/acetate buffer (10/90 v/v, pH 5.0) and in the O/W emulsion at Q concentration of 0.0034% w/w and 0.0084% w/w, respectively.

All the samples (10.0 mL) were placed at a distance of 10.0 cm from a G40T10E UVB lamp (Sankyo Denki) with 2.5×10^{-4} W cm^{-2} power irradiance. During illumination the samples were stirred by an IKA RO 5 multiple magnetic stirrer. At scheduled times up to 24 h, a fixed amount (200 µL) of each sample was withdrawn and properly diluted with ethanol for spectrophotometrical analysis. The photodegradation kinetics were studied by plotting the percentage of non-degraded Q as a function of irradiation time. The percentage of non-degraded Q was calculated as follows:

$$\% \text{ non-degraded Q} = C_t/C_0 \times 100$$

where C_0 is the Q concentration at zero time while C_t is the Q concentration after a given irradiation time (t). The study was carried out in triplicate.

2.6.4. Ex vivo experiments on porcine skin

Transepidermal permeation and skin uptake were determined using vertical Franz diffusion cells and porcine skin. Skin slices were isolated with an Acculan Aesculap dermatome from the outer side of pig ears freshly obtained from a local slaughterhouse and then stored for at least 24 h at -18 °C. Prior to each experiment, the excised skin was rinsed with normal saline solution and pre-hydrated by floating it in 0.002% (w/v) sodium azide aqueous solution. The skin was then sandwiched between the two cells with the *stratum corneum* side upwards. The receptor chamber

was filled with 6 mL of normal saline solution/ethanol (85/15 v/v) mixture.

An aliquot (500 µL) consisting of 0.091% w/v Q, free or complexed (Q/NH_2-MSN_1/1), in ethanol/acetate buffer (20/80 v/v, pH 5.0) was applied to the skin surface (available diffusion area of 1.60 cm^2). The same procedure was followed for the emulsion systems (O/W or W/O) containing 0.27% w/w of flavonoid. The content of the receptor chamber, continuously stirred at 34 ± 1 °C, was removed at appropriate intervals (1-24 h) for Q determination and the cell was immediately refilled with fresh receptor solution. At the end of the experiment, the application site of the skin was washed with normal saline solution (0.9% w/v sodium chloride) to remove the residual formulation on the surface. The skin was then cut with scalpel into small pieces and added with ethanol (2.0 mL) for Q extraction. After 24 h of magnetic stirring at RT, the resulting suspension was centrifuged and the supernatant was assayed by HPLC analysis. The skin uptake was expressed as Q amount *vs* skin diffusion area (µg/cm^2).

2.6.5. Cell proliferation assays

Cell growth inhibition was evaluated in JR8 melanoma cell line by sulforhodamine B colorimetric proliferation assay (SRB assay) [53], modified by Vichai and Kirtikara [54]. JR8 cells were routinely grown in RPMI-1640 added with 10% (v/v) fetal calf serum, 1% (v/v) penicillin-streptomycin, and maintained in standard conditions (37 °C, 5% CO_2 and 95% humidity).

For cell proliferation assays, Q, Q/NH_2-MSN_1/1, NH_2-MSN, MSN were pre-suspended in culture medium containing 1% (v/v) ethanol. Thirty thousand cells were seeded into 96-well plates. After 24 h, cells were incubated for 72 h, in triplicate wells, with the following, all diluted in culture medium: *i)* 1, 10, 30, 60 µM Q; *ii)* Q/NH_2-MSN_1/1 amounts, containing the same Q concentration as previously; *iii)* NH_2-MSN and MSN in the same amounts present in the complex.

Control cells were incubated with culture medium containing the same final concentration of ethanol (maximum concentration 0.5% v/v).

Incubation was stopped by addition of 0.1 mL/well of trichloroacetic acid (10% w/v solution). After 1 h at 4 °C, plates were washed repeatedly with water. The plates were then air-dried and stained with a 0.1 mL/well of SRB solution (0.057% w/v in 1% v/v acetic acid) (Sigma) for 30 min. Unbound dye was washed out four times with 0.2 mL/well of acetic acid (1% v/v). The SRB dye within cells was solubilized with 0.2 mL/well of Tris buffered saline (10 mM, pH 10.5) and optical density (OD) was quantified photometrically (492 nm) using a microplate reader Titertek Multiskan Plus (ICN Biomedical). The cell growth was expressed as percentage (mean OD of treated cells/mean OD of control cells $\times$100).

3. Results and discussion

Physico-chemical characterization

In this research the applicability of MSN as matrices for the topical release of Q was studied.

TGA was employed to measure the amount of functional groups (aminopropyl) and the final Q loading in the inclusion complexes. Typical thermograms of the Q/NH_2-MSN complexes are reported in Fig. 1 together with those of the parent NH_2-MSN and MSN materials. Comparison among the weight losses of the three types of materials allowed calculating the weight percentage of functional groups and included Q molecules, as described elsewhere [49, 50].

The loading capabilities of NH_2-MSN with different w/w ratios are listed in Table 1; Q complex with non-functionalized MSN was also considered for sake of comparison. This comparison clearly indicates that the storage ability of MSN is much lower than that of modified NH_2-MSN. However this property of NH_2-MSN does not increase with the Q amount employed in the preparation (w/w ratio). These results demonstrated the significant contribution of the aminopropyl-functionalization to drug uptake. The calculated values are in good agreement with Q quantification by UV-Vis spectrophotometry after extraction with absolute methanol (Table 1). These data were double

checked by measuring the Q amount remained in the supernatant (not reported). On the basis of these findings it can be stated that the complexation by 1/1 w/w ratio gave the most satisfactory results, thus for sake of brevity, the results description will be focused on this Q/NH_2-MSN complex.

Fig. 2 reports the low angle XRD patterns of Q/NH_2-MSN_1/1, NH_2-MSN and the parent MSN. Bare MSN shows the typical peaks due to an ordered hexagonal network of mesopores. The intensity of the peaks decreases after functionalization and subsequent Q loading (curves b and c, respectively), as often observed for this kind of materials. This trend could be interpreted in terms of pores filling with functional groups and Q molecules, while preserving the mesoporous structure [49, 50].

The HRTEM image of Q/NH_2-MSN_1/1 revealed the presence of nanosized mesoporous spheres, with an average particle size of ca. 250 (± 50) nm, characterized by regular and ordered channels with hexagonal symmetry (Fig. 3, Section A). The microscopic analyses confirmed that neither the grafting procedures nor the complexation phenomenon affected the structure and morphology of NH_2-MSN. This can be appreciated in the high magnification image in Fig. 3, Section B.

The low temperature nitrogen adsorption/desorption isotherms of the Q/NH_2-MSN_1/1 and NH_2-MSN samples are reported in Fig. 4, together with that of the parent MSN for comparison. All samples show the type IV isotherm typical of mesoporous materials. The decrease in the amount of nitrogen adsorbed by MSN to NH_2-MSN and Q/NH_2-MSN_1/1 is a clear indication of SSA decrease (see Table 2). This is also accompanied by changes in the curves shape, which accounts for modification of pore size and available volume [49, 50]. The data, in agreement with the other characterization techniques described above, suggest the lining of the pores with aminopropyl groups and their filling with Q molecules. This suggests a relatively strong interaction between functionalized silica and Q molecules.

FT-IR spectroscopy was employed to get information at the molecular level on the interaction of Q with the silica surface. The main vibrational modes of silica surface groups (silanols and

aminopropyls) and Q molecules are labeled in Fig. 5. A detailed analysis of the spectra (outside the scopes of this paper) confirms the presence and structural integrity of Q molecules within the silica pores. Moreover, changes in the position of Q vibrational modes (νC=O, aromatic νC=C and νC-O/δO-H combination modes, see Fig. 5) indicate hydrogen bonding interactions from the silica surface groups to the carbonyl of Q [55].

Regarding zeta potential measurements, as shown in Fig. S1, the value of MSN was -26.8 (± 0.56) mV, while it increased to +17.3 (± 0.46) mV after functionalization. This is because the silanol groups were negatively charged under a wide range pH conditions, while the aminopropyl groups attached on MSN were positively charged when suspended in water. This zeta potential variation well confirmed the successful functionalization of aminopropyl groups on MSN.

Upon Q loading, the zeta potential of MSN changed from -26.8 to -19.0 (± 0.81) mV while that of NH_2-MSN varied from +17.3 to +13.6 (± 0.16) mV indicating that probably antioxidant molecules, partially deposited on the surface of the silica nanoparticles, could shield their surface charge leading to decrease in zeta potential absolute values.

The interaction of Q with the aminopropyl-functionalized silica surface was further verified by DSC technique (not reported). NH_2-MSN did not display any peak while pure Q showed an intense endothermic peak at 321 °C characterized by ΔH = 148 J/g and related to the melting process. However, in the flavonoid complex this endothermic peak was suppressed indicating the molecular dispersion of Q within the silica pores. No differences are remarked among the complexes prepared in different weight ratios, suggesting the partial protection due to the encapsulation of Q within mesoporous silica and an important Q/silica molecular interaction for all the tested complexes.

Testing of complex properties

Diffusion tests through a semi-permeable membrane were carried out in order to assess Q release from the mesoporous matrices in topical formulations.

Results are summarized in Fig. 6 in terms of diffusion rate. Data indicated that both in ethanol/acetate buffer (20/80 v/v, pH 5.0) and in O/W emulsion the diffusion from the complex was delayed compared to that obtained from free Q confirming that a certain interaction between the two species occurred. The diffusion followed a pseudo-zero order kinetics both for pure Q and for the complex although the slopes of the O/W emulsion are lower than those of the solution. Besides, in both the tested media the diffusion rate of Q from the complex was quite evident confirming that no-covalent bonds were involved in the complex formation. Moreover, Q -either free or complexed with NH_2-MSN- diffused more slowly from O/W emulsion than from ethanol/acetate buffer, indicating that the polarity of the system can influence its release. Thus, it can be hypothesized that Q diffusion from complex is affected by both the dispersion system and the silica matrix.

Antioxidants like flavonoids are frequently used in sunscreen formulations to complement UV filter photoprotection by preventing or reducing the damage from the free radicals generated by solar radiation [56]. Anyway the photochemical instability of Q represents a limitation for its potential applicability in suncare products.

Initially investigations on the light-induced decomposition of Q were performed in an aqueous environment. Since Q is practically insoluble in water, it was solubilized in a hydroalcoholic solution of ethanol/acetate buffer (20/80, pH 5.0). The photodegradation curves were linearized and the rate equations are reported in Table 3. The percentage of the non-degraded flavonoid 24 h after UVB irradiation of the examined formulations was 52.6% for the non-encapsulated Q and 76.5% for the complexed one (Table 4). Although these studies provided valuable information on the photochemistry aspects, their relevance to the real conditions encountered in the use of topical preparations is limited. In order to overcome this drawback, in the present investigation the photochemical behavior of free and complexed Q was also examined using a cream (oil-in-water emulsion) as vehicle. This system was selected as a model formulation since it represents the most common type of topical preparation and hence reproduces the actual applicative conditions of

dermatological products. Moreover it was reported that Q photodegradation was observed in creams, unless protected in lipid droplets [57].

In the present emulsion, pure Q showed a degradation of 11.7% meanwhile the complexed Q irradiated at the same conditions exhibited no meaningful alteration in the percentage content over the monitoring period. The molecular photostability of the Q is substantially enhanced compared to the solution samples stored in the same conditions, proving that the presence of a biphasic system could significantly increase the flavonoid photostability. It could be concluded from these findings that the simultaneous inclusion in NH_2-MSN and the dispersion in an emulsion system would be an effective route to improve the stabilization of the chemical labile drugs. Q photostability is of crucial importance because it was demonstrate that among the hydroxyl groups in Q, those in position 3, 3' and 4' are mainly involved in the antioxidant activity of the compound, as well as in its photolability [58]. In this way not only Q stability increased but also antioxidant ability could noticeably be potentiated.

Topical delivery of quercetin

Due to the well-documented antioxidant properties of Q and its safety on normal cells, an utilize of this compound in topical formulations, as protective agent, could be envisaged. Although the active ingredient of pharmaceutical or personal care products is essential, the method and the vehicle in which it is delivered are crucial. Micro- and nanoparticulate systems, including microspheres and nanoparticles, are used to make substances more compatible with each other, to release the active in a controlled manner and also to protect from degradative phenomena. Some vehicles not only stabilize the active ingredients, but also enhance their delivery across skin.

As a preliminary test for the possible use of these mesoporous nanoparticles as topical vectors for Q, an *ex vivo* study on porcine skin was performed. The choice of this model skin is due to its high affinity with the human one [59].

The experiments were carried out employing either the hydroalcoholic solution (ethanol/acetate buffer (20/80 v/v, pH 5.0) or the W/O emulsion as dispersion system for the Q-loaded silica nanoparticles. The corresponding free Q formulations were examined as controls.

Such studies are also relevant investigating topical drug delivery to make sure that none of the compounds appears to permeate transdermally. In our experiments, sampling was performed from the receptor media after 24 h to determine if there was a transdermal delivery of Q. All the studied systems showed a negligible transepidermal permeation; this observation is consistent with reports from other skin permeation studies of Q [60, 61].

The absence of transdermal delivery of Q can be attributed both to the barrier properties of the *stratum corneum* and to the structure and physico-chemical characteristics of this flavonoid. Indeed, one of the reasons contributing to the inability of Q to penetrate the skin could be its poor lipophilicity [62] and rather limited aqueous solubility [63].

Fig. 7 shows the amount of Q quantified in the skin 24 h after the application. Regarding free Q, different accumulation values were observed depending on the employed dispersion medium. Particularly, significant results were obtained with hydroalcoholic solution (3.36 μg/cm^2) and even more with the W/O emulsion (4.77 μg/cm^2). In contrast the accumulation observed from the O/W emulsion (data not shown) was almost negligible; therefore this system was excluded in the case of the complex sample. These results can be explained on the basis of the octanol-water partition coefficient (log P) of Q which is reported to be 1.82 thus unfavorable to water which is the external phase of this medium [64].

The silica-based formulations showed higher amounts of Q retained in the skin (9.79 μg/cm^2 from hydroalcoholic solution and 10.89 μg/cm^2 from W/O emulsion) compared to those containing free Q. The improved skin accumulation observed from the nanosized complex could derived from an increased contact surface with the corneocytes. Specifically, due to the electrostatic interaction with the negatively charged character of the cell membranes, the positive surface charge of the mesoporous nanocarriers could favour adhesion to the upper skin layers, prolonging the release and

enhancing the bioavailability of the included active molecule. All these reasons could contribute to the increased ability of Q immobilized in nanoparticles to greater accumulate into the skin, as already demonstrated in our previous study on rutin [49].

Skin penetration and drug localization are the main goals of topically administered products. Nevertheless, the outer skin layer (*stratum corneum*) is characterized by a highly hydrophobic lipid matrix primarily consisting of ceramides, cholesterol and fatty acids and consequently it has the rare ability to block both the hydrophilic and hydrophobic penetrants. Ideally, topically applied formulations are designed to penetrate the skin to a certain degree, to achieve a significant residence time, and to deliver an active compound, all the while remaining non-irritating.

Thus, particles must be rationally designed to penetrate beyond the *stratum corneum* and persist within the skin despite routine washing and natural skin sloughing. Small particle size has been indicated by several studies to increase penetration within skin models [65]. In particular, for nanoparticles, an enhanced follicular penetration has been described whereas intercellular penetration for larger particles is hardly realistic due to their size [66]. However, up to now, most of the studies assessing the skin penetration of different nanoparticle types after topical application have shown penetration of particles into upper layers of the skin but not deeper into the viable epidermis and dermis.

Although we currently have no direct evidence for the localization of Q-loaded silica nanoparticles within the skin it can be reasonably suggested the feasibility of using this innovative carrier, especially vehicled in a W/O emulsion, to target active ingredients to corneocytes in order to prevent oxidative damages.

Cytotoxicity study on JR8 cell line

In addition to the antioxidant and scavenging ROS properties, that make Q suitable as skin protective in topical formulations, Q shows antiproliferative, cytotoxic, proapoptotic activities in a number of cancer cell lines of different origin (prostate, cervical, lung, breast, colon), included

melanoma cells [11-17].

Q is able to inhibit the growth and proliferation preferentially in cancer cells *versus* their normal counterparts through a process involving the down-regulation of selective oncogenes (such as Mcl-1, Ras, MEK, PI3K), or the up-regulation of tumor suppressor genes (p53, p21), which, in turn, enhance selective pathways leading to the elimination of cancer cells.

In order to check if the functionalized nanosized complex is a good delivery system of Q with the aim of inhibiting cell proliferation, the cytotoxic effect of the Q immobilized in silica nanoparticles, compared to free Q, was tested on a line of human melanoma cells.

The JR8 human melanoma cells were incubated with different concentrations, in the range 1 to 60 μM, of both free Q and Q/NH_2-MSN_1/1 for 72 h and the cell proliferation was determined by SRB assay, a method developed by Skehan and colleagues in 1990 at the National Cancer Institute (NCI) for high-throughput drug screening to measure drug-induced cytotoxicity and cell proliferation. Its principle is based on the ability of the protein dye sulforhodamine B to bind to protein basic amino acid residues of trichloroacetic acid-fixed cells. SRB assay provides linearity with cell number, high sensitivity and the staining is not cell-line-dependent [53].

The cytotoxicity of free and NH_2-MSN-complexed Q was compared with that of the same concentrations of both bare MSN and NH_2-MSN. As shown in Fig. 8, the proliferation of JR8 human melanoma cells was not affected by MSN and NH_2-MSN at the highest concentrations tested, suggesting that the nanoparticles used in this study show absence of toxicity and good biocompatibility. Free Q and Q/NH_2-MSN_1/1 complex at the lower tested concentration (1, 10, 30 μM) did not influence cell proliferation. However, by increasing the concentration of Q to 60 μM, cell growth inhibition, compared to untreated controls, was noticed. At this concentration the cell proliferation was inhibited of about 15 and 50% when the cells were treated respectively with Q or Q/NH_2-MSN_1/1. Our data are in agreement with the effect assessed in a different line of melanoma cells, the OCM-1, where a concentration 70 μM was found effective in blocking the proliferation and arresting cells at the G1 phase by inhibiting Cdk2 activity and up-regulating p27

and p21 [11].

Growth inhibition at concentrations ranging from 50 µM to 100 µM was also observed in different cancer cell lines [9, 67, 68], while the toxicity of Q in normal, non tumor cells, was detected at concentrations higher than 100 µM [10].

Our study underlines a higher cytotoxicity of Q when complexed with mesoporous silica nanoparticles, possibly due to a better release or cellular uptake by the nanosized system while the nanoparticles alone show no toxicity at higher concentration.

The potential application of Q formulations in cancer chemoprevention is based on its ability of inhibiting cell proliferation of cancer cells rather than normal ones. Cancer cell lines appear more susceptible to cycle arrest and apoptosis at concentration that have no or little effect on non-transformed cells. In this study a preliminary evaluation of cell growth inhibition by Q immobilized in NH_2-MSN was made in JR8 melanoma cell line: the positive obtained results stimulate further studies on different cell lines, both normal and tumoral, aimed to a better understanding of the mechanism of these nanocarriers-induced effects on the regulation of tumor growth.

CONCLUSIONS

A novel approach to improve the topical delivery of Q by immobilization in NH_2-MSN was demonstrated.

Different techniques were employed to establish the host/guest interaction between this flavonoid and mesoporous silica nanoparticles. The influence of the functionalization of the inorganic matrix on the Q bioactivity was also investigated.

The presence of aminopropyl groups lining the silica pores was confirmed by many characterization techniques, namely specific surface area and porosity analysis, XRD, TGA, HRTEM and zeta potential measurements. Q inclusion was determined both from a quantitative point of view (TGA,

spectrophotometric analysis) and from a molecular point of view by FT-IR spectroscopy. The latter proved the structural integrity of the molecules and gave hints on the hydrogen-bonding interaction of Q with the hybrid organic/inorganic surface.

Transmembrane diffusion study confirmed a certain host/guest interaction. The immobilization in NH_2-MSN improved the photostability of Q and the protective effect was more evident when the nanosized complex was dispersed in a biphasic system. The grafting of aminopropyl groups in the mesoporous silica resulted a valid strategy to increase Q penetration into the skin as can be deduced from the results obtained by the *ex vivo* porcine skin experiments.

These positive findings indicate that NH_2-MSN can be considered a potential topical carrier for encapsulating flavonoids derivatives improving their intrinsic stability and biological activity after topical application.

The cytotoxicity studies, albeit very preliminary, show that these Q-loaded mesoporous nanoparticles appear a very promising approach to deliver flavonoids as chemopreventive agents into targeted organs and cells; particularly they showed both a good biocompatibility and the ability to increase the antiproliferative activity of Q.

Since this is a preliminary screening study, *in vivo* testing needs to be conducted in future to demonstrate the applicability of this innovative delivery system.

Acknowledgements

Compagnia di San Paolo and Università degli Studi di Torino are gratefully acknowledged for funding Project ORTO114XNH through ‘‘Bando per il finanziamento di progetti di ricerca di Ateneo - anno 2011’’

This research has been carried out with the financial support of the University of Torino [Fondi di Ricerca Locale (ex 60%) 2012, 2013] and was supported by the European COST Action MP1202

“Rational design of hybrid organic inorganic interfaces: the next step towards advanced functional materials”.

References

[1] W. Lian, W. Bo, L. Hao, L. Huchen, Q. Fang, X. Lei, X. Yanhui, W. Gaoming, L. Xiaolong, W. Haiwei, H. J., Quercetin, a flavonoid with anti-inflammatory activity, suppresses the development of abdominal aortic aneurysms in mice., European Journal of Pharmacology, 690 (2012) 133-141.

[2] B. Romano, E. Pagano, V. Montanaro, A.L. Fortunato, N. Milic, F. Borrelli, Novel Insights into the Pharmacology of Flavonoids, Phytother. Res., 27 (2013) 1588-1596.

[3] C. Kandaswami, E.J. Middleton, Free radical scavenging and antioxidant activity of plant flavonoids, Adv. Exp. Med. Biol., 366 (1994) 351-376.

[4] W. Bors, W. Heller, C. Michel, M. Saran, Flavonoids as antioxidants - determination of radical-scavenging efficiencies, Methods Enzymol., 186 (1990) 343-355.

[5] W. Bors, C. Michel, M. Saran, Flavonoid antioxidants - rate constants for reactions with oxygen radicals, Oxyg. Radic. Biol. Syst. D, 234 (1994) 420-429.

[6] E.L. da Silva, M.K. Piskula, N. Yamamoto, J.H. Moon, J. Terao, Quercetin metabolites inhibit copper ion-induced lipid peroxidation in rat plasma, FEBS Lett., 430 (1998) 405-408.

[7] E. Vulcain, P. Goupy, C. Caris-Veyrat, O. Dangles, Inhibition of the metmyoglobin-induced peroxidation of linoleic acid by dietary antioxidants: Action in the aqueous vs. lipid phase, Free Radical Res., 39 (2005) 547-563.

[8] S. Bose, Y. Du, P. Takhistov, B. Michniak-Kohn, Formulation optimization and topical delivery of quercetin from solid lipid based nanosystems, Int. J. Pharm., 441 (2013) 56-66.

[9] A. Robaszkiewicz, A. Balcerczyk, G. Bartosz, Antioxidative and prooxidative effects of quercetin on A549 cells, Cell Biology International, 31 (2007) 1245-1250.

[10] L. Gibellini, M. Pinti, M. Nasi, J.P. Montagna, S. De Biasi, E. Roat, L. Bertoncelli, E.L. Cooper, A. Cossarizza, Quercetin and Cancer Chemoprevention, Evid.-based Complement Altern. Med., (2011) 1-15.

[11] M. Russo, C. Spagnuolo, I. Tedesco, S. Bilotto, G.L. Russo, The flavonoid quercetin in disease prevention and therapy: Facts and fancies, Biochem. Pharmacol., 83 (2012) 6-15.

[12] E. Braganhol, L.L. Zamin, A. Delgado Canedo, F. Horn, A.S.K. Tamajusuku, M.R. Wink, C. Salbego, A.M.O. Battastini, Antiproliferative effect of quercetin in the human U138MG glioma cell line, Anti-Cancer Drugs, 17 (2006) 663-671.

[13] R.V. Priyadarsini, R.S. Murugan, S. Maitreyi, K. Ramalingam, D. Karunagaran, S. Nagini, The flavonoid quercetin induces cell cycle arrest and mitochondria-mediated apoptosis in human cervical cancer (HeLa) cells through p53 induction and NF-kappa B inhibition, Eur. J. Pharmacol., 649 (2010) 84-91.

[14] E.J. Choi, S.M. Bae, W.S. Ahn, Antiproliferative Effects of Quercetin through Cell Cycle Arrest and Apoptosis in Human Breast Cancer MDA-MB-453 Cells, Arch. Pharmacal Res., 31 (2008) 1281-1285.

[15] S. Priego, F. Feddi, P. Ferrer, S. Mena, M. Benlloch, A. Ortega, J. Carretero, E. Obrador, M. Asensi, J.M. Estrela, Natural polyphenols facilitate elimination of HT-29 colorectal cancer xenografts by chemoradiotherapy: a Bcl-2-and superoxide dismutase 2-dependent mechanism, Mol. Cancer Ther., 7 (2008) 3330-3342.

[16] J. Duraj, K. Zazrivcova, J. Bodo, M. Sulikova, J. Sedlak, Flavonoid quercetin, but not apigenin or luteolin, induced apoptosis in human myeloid leukemia cells and their resistant variants, Neoplasma, 52 (2005) 273-279.

[17] J.W. Kang, J.H. Kim, K. Song, S.H. Kim, J.-H. Yoon, K.-S. Kim, Kaempferol and Quercetin, Components of Ginkgo biloba Extract (EGb 761), Induce Caspase-3-Dependent Apoptosis in Oral Cavity Cancer Cells, Phytother. Res., 24 (2010) S77-S82.

[18] J.H. Yang, T.C. Hsia, H.M. Kuo, P.D.L. Chao, C.C. Chou, Y.H. Wei, J.G. Chung, Inhibition of lung cancer cell growth by quercetin glucuronides via G(2)/M arrest and induction of apoptosis, Drug Metab. Dispos., 34 (2006) 296-304.

[19] T.-J. Lee, O.H. Kim, Y.H. Kim, J.H. Lim, S. Kim, J.-W. Park, T.K. Kwon, Quercetin arrests G2M phase and induces caspase-dependent cell death in U937 cells, Cancer Lett., 240 (2006) 234-242.

[20] J.A. Choi, J.Y. Kim, J.Y. Lee, C.M. Kang, H.J. Kwon, Y.D. Yoo, T.W. Kim, Y.S. Lee, S.J. Lee, Induction of cell cycle arrest and apoptosis in human breast cancer cells by quercetin, Int. J. Oncol., 19 (2001) 837-844.

[21] C.S. Ong, E. Tran, T.T.T. Nguyen, C.K. Ong, S.K. Lee, J.J. Lee, C.P. Ng, C. Leong, H. Huynh, Quercetin-induced growth inhibition and cell death in nasopharyngeal carcinoma cells are associated with increase in Bad and hypophosphorylated retinoblastoma expressions, Oncol. Rep., 11 (2004) 727-733.

[22] R.G. Beniston, M.S. Campo, Quercetin elevates p27(Kip1) and arrests both primary and HPV16 E6/E7 transformed human keratinocytes in G1, Oncogene, 22 (2003) 5504-5514.

[23] M. Yoshizumi, K. Tsuchiya, K. Kirima, M. Kyaw, Y. Suzaki, T. Tamaki, Quercetin inhibits Shc- and phosphatidylinositol 3-kinase-mediated c-Jun N-terminal kinase activation by angiotensin II in cultured rat aortic smooth muscle cells, Mol. Pharmacol., 60 (2001) 656-665.

[24] M.E. Carlotti, S. Sapino, E. Ugazio, G. Caron, On the complexation of quercetin with methyl-beta-cyclodextrin: photostability and antioxidant studies, J. Incl. Phenom. Macrocycl. Chem., 70 (2011) 81-90.

[25] F. Puoci, C. Morelli, G. Cirillo, M. Curcio, O.I. Parisi, P. Maris, D. Sisci, N. Picci, Anticancer Activity of a Quercetin-based Polymer Towards HeLa Cancer Cells, Anticancer Res., 32 (2012) 2843-2847.

[26] Y. Zhang, Y. Yang, K. Tang, X. Hu, G. Zou, Physicochemical characterization and antioxidant activity of quercetin-loaded chitosan nanoparticles, J. Appl. Polym. Sci., 107 (2008) 891-897.

[27] P.G. Cadena, M.A. Pereira, R.B.S. Cordeiro, I.M.F. Cavalcanti, B. Barros Neto, M.d.C.C.B. Pimentel, J.L. Lima Filho, V.L. Silva, N.S. Santos-Magalhaes, Nanoencapsulation of quercetin and resveratrol into elastic liposomes, Biochim. Biophys. Acta-Biomembr., 1828 (2013) 309-316.

[28] M. Vallet-Regí, A. Rámila, R.P. del Real, J. Pérez-Pariente, A New Property of MCM-41: Drug Delivery System, Chem. Mater., 13 (2001) 308-311.

[29] D.P. Ferris, Y.-L. Zhao, N.M. Khashab, H.A. Khatib, J.F. Stoddart, J.I. Zink, Light-Operated Mechanized Nanoparticles, J. Am. Chem. Soc., 131 (2009) 1686-1688.

[30] M.W. Ambrogio, C.R. Thomas, Y.-L. Zhao, J.I. Zink, J.F. Stoddart, Mechanized Silica Nanoparticles: A New Frontier in Theranostic Nanomedicine, Acc. Chem. Res., 44 (2011) 903-913.

[31] T. Fontecave, C. Sanchez, T. Azais, C. Boissiere, Chemical Modification As a Versatile Tool for Tuning Stability of Silica Based Mesoporous Carriers in Biologically Relevant Conditions, Chem. Mater., 24 (2012) 4326-4336.

[32] Z. Li, J.C. Barnes, A. Bosoy, J.F. Stoddart, J.I. Zink, Mesoporous silica nanoparticles in biomedical applications, Chem. Soc. Rev., 41 (2012) 2590-2605.

[33] J. Andersson, J. Rosenholm, S. Areva, M. Linden, Influences of material characteristics on ibuprofen drug loading and release profiles from ordered micro- and mesoporous silica matrices, Chem. Mater., 16 (2004) 4160-4167.

[34] V. Cauda, L. Muehlstein, B. Onida, T. Bein, Tuning drug uptake and release rates through different morphologies and pore diameters of confined mesoporous silica, Microporous Mesoporous Mater., 118 (2009) 435-442.

[35] M. Vallet-Regí, F. Balas, D. Arcos, Mesoporous materials for drug delivery, Angew. Chem. Int. Edit., 46 (2007) 7548-7558.

[36] M. Manzano, M. Colilla, M. Vallet-Regí, Drug delivery from ordered mesoporous matrices, Expert Opin. Drug Deliv., 6 (2009) 1383-1400.

[37] V. Cauda, B. Onida, B. Platschek, L. Muehlstein, T. Bein, Large antibiotic molecule diffusion in confined mesoporous silica with controlled morphology, J. Mater. Chem., 18 (2008) 5888-5899.

[38] V. Ambrogi, L. Perioli, C. Pagano, F. Marmottini, M. Moretti, F. Mizzi, C. Rossi, Econazole Nitrate-Loaded MCM-41 for an Antifungal Topical Powder Formulation, J. Pharm. Sci., 99 (2010) 4738-4745.

[39] L. Gastaldi, E. Ugazio, S. Sapino, P. Iliade, I. Miletto, G. Berlier, Mesoporous silica as a carrier for topical application: the Trolox case study, PCCP, 14 (2012) 11318-11326.

[40] V. Ambrogi, L. Latterini, F. Marmottini, C. Pagano, M. Ricci, Mesoporous silicate MCM-41 as a particulate carrier for octyl methoxycinnamate: Sunscreen release and photostability, J. Pharm. Sci., 102 (2013) 1468-1475.

[41] A.J. Di Pasqua, K.K. Sharma, Y.-L. Shi, B.B. Toms, W. Ouellette, J.C. Dabrowiak, T. Asefa, Cytotoxicity of mesoporous silica nanomaterials, J. Inorg. Biochem., 102 (2008) 1416-1423.

[42] A. Garcia, M. Colilla, I. Izquierdo-Barba, M. Vallet-Regí, Incorporation of Phosphorus into Mesostructured Silicas: A Novel Approach to Reduce the SiO_2 Leaching in Water, Chem. Mater., 21 (2009) 4135-4145.

[43] X. Huang, X. Teng, D. Chen, F. Tang, J. He, The effect of the shape of mesoporous silica nanoparticles on cellular uptake and cell function, Biomaterials, 31 (2010) 438-448.

[44] Y.-S. Lin, N. Abadeer, C.L. Haynes, Stability of small mesoporous silica nanoparticles in biological media, Chem. Commun., 47 (2011) 532-534.

[45] J. Lu, M. Liong, Z. Li, J.I. Zink, F. Tamanoi, Biocompatibility, Biodistribution, and Drug-Delivery Efficiency of Mesoporous Silica Nanoparticles for Cancer Therapy in Animals, Small, 6 (2010) 1794-1805.

[46] R. Mortera, S. Fiorilli, E. Garrone, E. Verne, B. Onida, Pores occlusion in MCM-41 spheres immersed in SBF and the effect on ibuprofen delivery kinetics: A quantitative model, Chem. Eng. J., 156 (2010) 184-192.

[47] Z. Tao, M.P. Morrow, T. Asefa, K.K. Sharma, C. Duncan, A. Anan, H.S. Penefsky, J. Goodisman, A.-K. Souid, Mesoporous silica nanoparticles inhibit cellular respiration, Nano Lett., 8 (2008) 1517-1526.

[48] B. Trewyn, J. Nieweg, Y. Zhao, V. Lin, Biocompatible mesoporous silica nanoparticles with different morphologies for animal cell membrane penetration, Chem. Eng. J., 137 (2008) 23-29.

[49] G. Berlier, L. Gastaldi, S. Sapino, I. Miletto, E. Bottinelli, D. Chirio, E. Ugazio, MCM-41 as a useful vector for rutin topical formulations: Synthesis, characterization and testing, Int. J. Pharm., 457 (2013) 177-186.

[50] G. Berlier, L. Gastaldi, E. Ugazio, I. Miletto, P. Iliade, S. Sapino, Stabilization of quercetin flavonoid in MCM-41 mesoporous silica: positive effect of surface functionalization, J. Colloid Interface Sci., 393 (2013) 109-118.

[51] D.R. Radu, C.Y. Lai, K. Jeftinija, E.W. Rowe, S. Jeftinija, V.S.Y. Lin, A polyamidoamine dendrimer-capped mesoporous silica nanosphere-based gene transfection reagent, J. Am. Chem. Soc., 126 (2004) 13216-13217.

[52] D. Tarn, M. Xue, J.I. Zink, pH-Responsive Dual Cargo Delivery from Mesoporous Silica Nanoparticles with a Metal-Latched Nanogate, Inorg. Chem., 52 (2013) 2044-2049.

[53] P. Skehan, R. Storeng, D. Scudiero, A. Monks, J. McMahon, D. Vistica, J.T. Warren, H. Bokesch, S. Kenney, M.R. Boyd, New colorimetric cytotoxicity assay for anticancer-drug screening, JNCI-J. Natl. Cancer Inst., 82 (1990) 1107-1112.

[54] V. Vichai, K. Kirtikara, Sulforhodamine B colorimetric assay for cytotoxicity screening, Nat. Protoc., 1 (2006) 1112-1116.

[55] G. Socrates, Infrared and Raman characteristic group frequencies, Ed., John Wiley & Sons Ltd, Chichester, England, 2006.

[56] S. Scalia, M. Mezzena, Photostabilization Effect of Quercetin on the UV Filter Combination, Butyl Methoxydibenzoylmethane-Octyl Methoxycinnamate, Photochem. Photobiol., 86 (2010) 273-278.

[57] G.J. Smith, S.J. Thomsen, K.R. Markham, C. Andary, D. Cardon, The photostabilities of naturally occurring 5-hydroxyflavones, flavonols, their glycosides and their aluminium complexes, J. Photochem. Photobiol. A, 136 (2000) 87-91.

[58] S. Dall'Acqua, G. Miolo, G. Innocenti, S. Caffieri, the photodegradation of quercetin: relation to oxidation, Molecules, 17 (2012) 8898-8907.

[59] N. Sekkat, Y.N. Kalia, R.H. Guy, Biophysical study of porcine ear skin in vitro and its comparison to human skin in vivo, J. Pharm. Sci., 91 (2002) 2376-2381.

[60] S. Kitagawa, Y. Tanaka, M. Tanaka, K. Endo, A. Yoshii, Enhanced skin delivery of quercetin by microemulsion, J. Pharm. Pharmacol., 61 (2009) 855-860.

[61] F.T.M.C. Vicentini, T.R.M. Simi, J.O. Del Ciampo, N.O. Wolga, D.L. Pitol, M.M. Iyomasa, M.V.L.B. Bentley, M.J.V. Fonseca, Quercetin in w/o microemulsion: In vitro and in vivo skin penetration and efficacy against UVB-induced skin damages evaluated in vivo, Eur. J. Pharm. Biopharm., 69 (2008) 948-957.

[62] L. Montenegro, C. Carbone, C. Maniscalco, D. Lambusta, G. Nicolosi, C.A. Ventura, G. Puglisi, In vitro evaluation of quercetin-3-O-acyl esters as topical prodrugs, Int. J. Pharm., 336 (2007) 257-262.

[63] F. Bonina, M. Lanza, L. Montenegro, C. Puglisi, A. Tomaino, D. Trombetta, F. Castelli, A. Saija, Flavonoids as potential protective agents against photo-oxidative skin damage, Int. J. Pharm., 145 (1996) 87-94.

[64] J.A. Rothwell, A.J. Day, M.R.A. Morgan, Experimental determination of octanol-water partition coefficients of quercetin and related flavonoids, J. Agric. Food Chem., 53 (2005) 4355-4360.

[65] F. Rancan, Q. Gao, C. Graf, S. Troppens, S. Hadam, S. Hackbarth, C. Kembuan, U. Blume-Peytavi, E. Rühl, J. Lademann, A. Vogt, Skin penetration and cellular uptake of amorphous silica nanoparticles with variable size, surface functionalization, and colloidal stability, ACS Nano, 8 (2012) 6829-6842.

[66] J. Lademann, H. Richter, A. Teichmann, N. Otberg, U. Blume-Peytavi, J. Luengo, B. Weiss, U.F. Schaefer, C.-M. Lehr, R. Wepf, W. Sterry, Nanoparticles - An efficient carrier for drug delivery into the hair follicles, Eur. J. Pharm. Biopharm., 66 (2007) 159-164.

[67] M. Alia, R. Mateos, S. Ramos, E. Lecumberri, L. Bravo, L. Goya, Influence of quercetin and rutin on growth and antioxidant defense system of a human hepatoma cell line (HepG2), Eur. J. Nutr., 45 (2006) 19-28.

[68] J. Chen, Y.X. Ou, W.M. Da, J.H. Kang, Coadjustment of quercetin and hydrogen peroxide: the role of ROS in the cytotoxicity of quercetin, Pharmazie, 59 (2004) 155-158.

Table 1. Data from thermogravimetric analysis (percentage weight loss) and from UV-Vis spectrophotometric analysis (percentage of loading, % wt Q)

		Quercetin	
Samples	Aminopropyl groups	TGA	UV-Vis
MSN	-	-	-
NH_2-MSN	10.2	-	-
Q/MSN_1/1	-	4.7	3.2
Q/NH_2-MSN_1/1	10.2	9.2	8.0
Q/NH_2-MSN_1/3	9.6	8.3	6.0
Q/NH_2-MSN_3/1	9.6	9.5	8.0

Table 2. Porosity and specific surface area of the silica based samples

Samples	Pore diameter (Å)	SSA ($m^2 \cdot g^{-1}$)	Pore Volume ($cm^3 \cdot g^{-1}$)
MSN	32	1216	1.98
NH_2-MSN	27	704	0.85
Q/NH_2-MSN_1/1	-	90	0.25

Table 3. Photodegradation equations of Q, free or complexed with silica in 1/1 w/w ratio, in ethanol/acetate buffer (20/80 v/v, pH 5.0) or in O/W emulsion (pH 5.0), upon UVB irradiation (24 h).

Samples	Solution		O/W emulsion	
Q	y = -1.975x + 100.0	R^2= 0.970	y = -0.467x + 99.5	R^2= 0.995
Q/NH_2-MSN_1/1	y = -0.979x + 100.0	R^2= 0.910	y = -0.049x + 100.1	R^2= 0.963

Table 4. Percentage of non-degraded Q, free or complexed with silica in 1/1 w/w ratio, in ethanol/acetate buffer (20/80 v/v, pH 5.0) or in O/W emulsion (pH 5.0), upon UVB irradiation (24 h).

	% non-degraded Q	
Samples	Solution	O/W emulsion
Q	52.6 (± 3.6)	88.3 (± 1.6)
Q/NH_2-MSN_1/1	76.5 (± 2.1)	98.9 (± 1.8)

Table S1. Percent composition of O/W emulsion

Ingredients	% wt
Phytocream® 2000	2.5
Tegosoft® CI	6.5
Abil® 350	1.0
Carbopol® ETD 2001	0.1
Glycerol	4.5
Water	85.4

Table S2. Percent composition of W/O emulsion

Ingredients	% wt
Arlacel® P135	2.0
Tegosoft® CT	9.0
Isopropyl myristate	9.0
Glycerol	4.0
Magnesium sulfate	0.7
Water	75.3

Figure captions:

Scheme 1. Structure of quercetin molecule

Fig. 1. Thermogravimetric analysis of MSN (a), NH_2-MSN (b) and Q/NH_2-MSN_1/1 (c). Weight losses were measured in N_2 flow up to 1000 °C, and in air for a 15 min isotherm at the same temperature.

Fig. 2. Powder XRD patterns of a MSN (a), NH_2-MSN (b) and Q/ NH_2-MSN_1/1 (c).

Fig 3. Representative HRTEM images of the Q/NH_2-MSN_1/1: 30000X (A); 120000X (B).

Fig. 4. Nitrogen isotherm adsorption (□) and desorption (×) on MSN (a), NH_2-MSN (b) and Q/NH_2-MSN_1/1 (c).

Fig. 5. FT-IR spectra of NH_2-MSN, Q/NH_2-MSN_1/1 and free Q in the high and low frequency ranges (top and bottom, respectively).

Fig. 6. Diffusion profiles of Q in ethanol/acetate buffer (20/80, pH 5.0) solution (black solid line, diamond), Q in O/W emulsion (black dotted line, square), Q/NH_2-MSN_1/1 in ethanol/acetate buffer pH 5.0 (20/80) solution (grey solid line, triangle) and Q/NH_2-MSN_1/1 in O/W emulsion (grey dotted line, cross) through the cellulose membrane. Each bar represents the mean ± SD obtained in three independent experiments.

Fig. 7. *Ex vivo* porcine skin accumulation values of free Q (black) and Q/NH_2-MSN_1/1 (grey) 24 h after application on Franz diffusion cells from different media. Each bar represents the mean ± SD obtained in three independent experiments.

Fig. 8. Effect of Q, Q/NH_2-MSN_1/1, NH_2-MSN and MSN on JR8 cell proliferation by SRB assay. Cells were incubated with the substances at different concentrations for 72 h. The concentration of silica nanoparticles is shown in the upper axis, while the concentration of Q, both free or complexed, is reported in the lower axis. Cell growth is expressed as % T/C (mean OD of treated cells/mean OD of control cells ×100). Values are mean ± SD (n=3 wells/condition) of two independent experiments**.**

Fig. S1. Effect of aminopropyl functionalization and Q loading on zeta potential of MSN

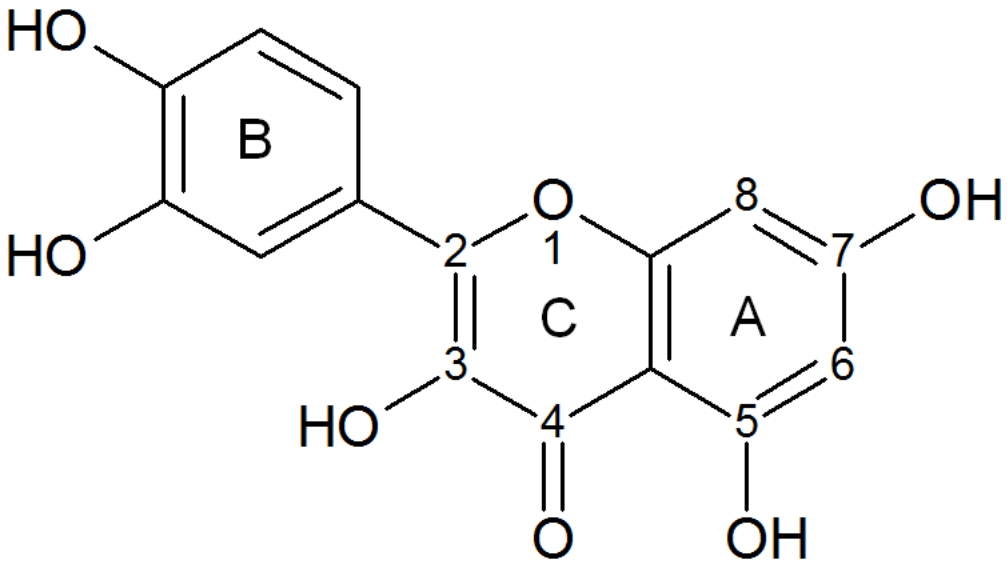

Scheme 1

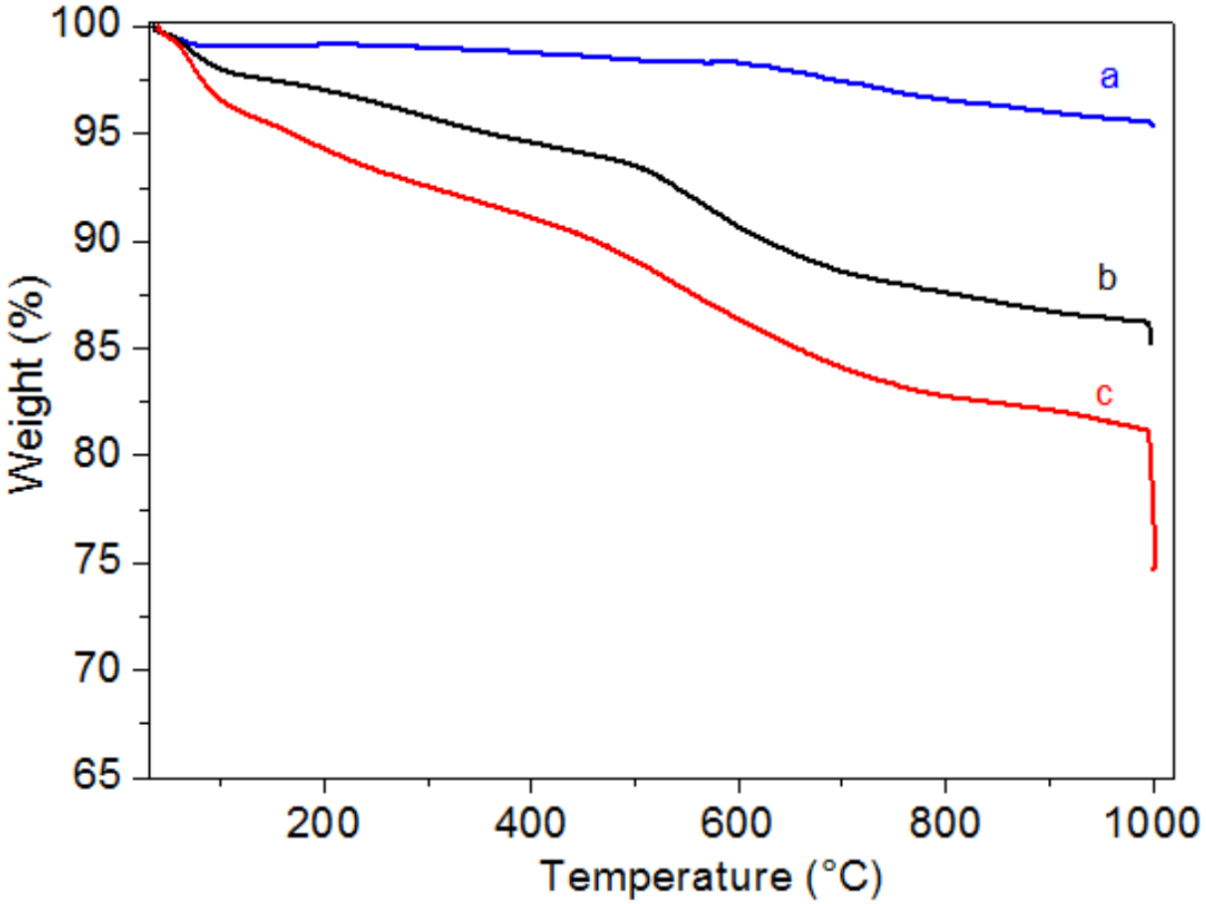
100
95
90
85
80
75
70
65
Weight (%)
200
400
600
800
1000
Temperature (°C)
a
b
c

Fig. 1

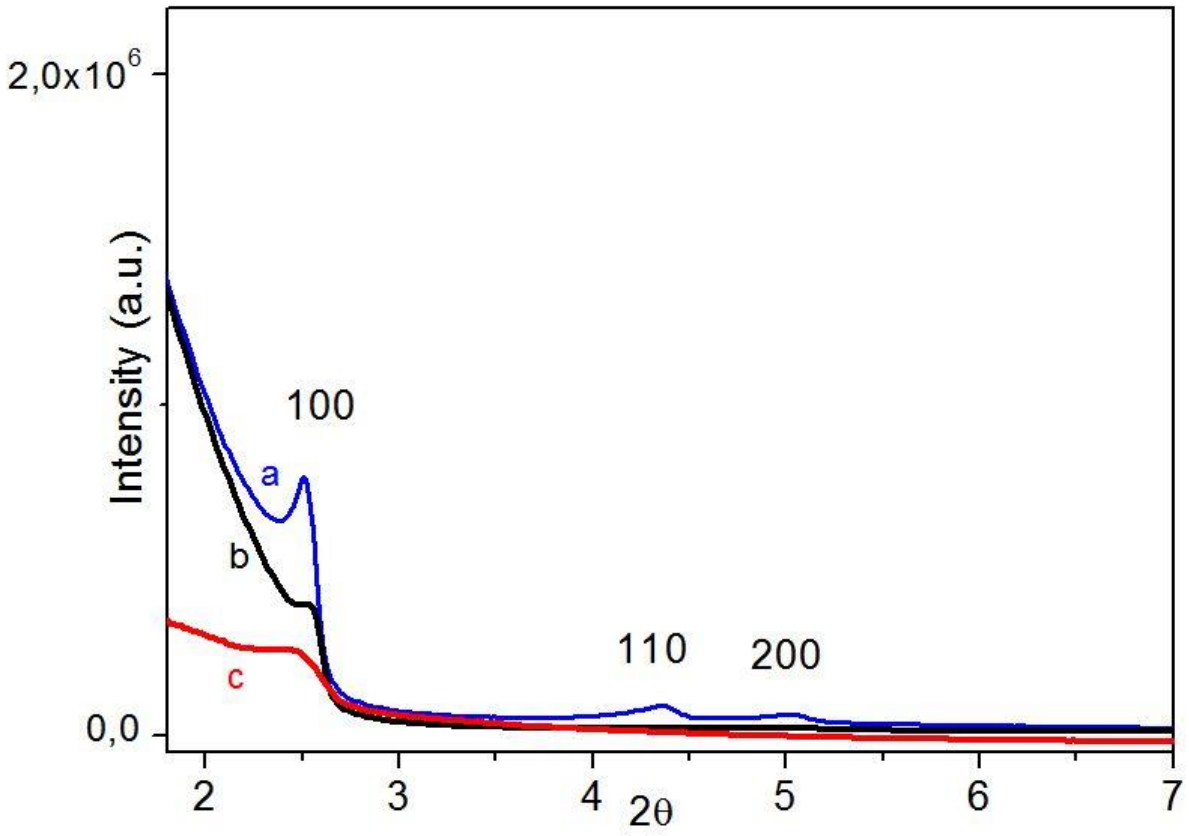

Fig. 2

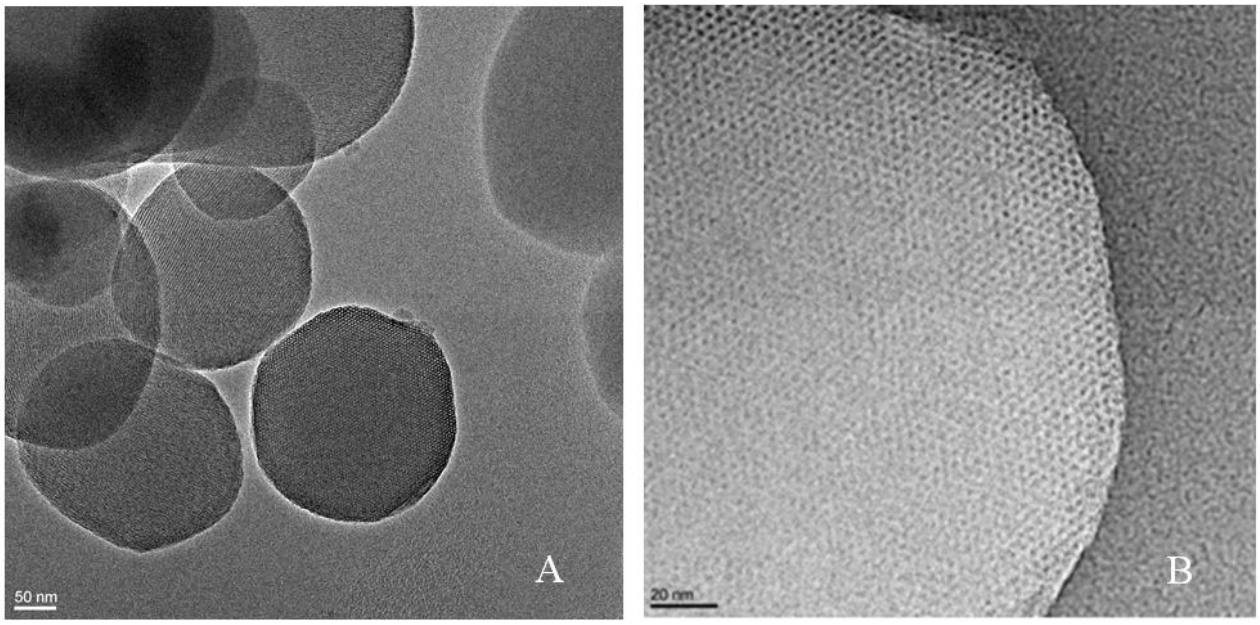

Fig. 3

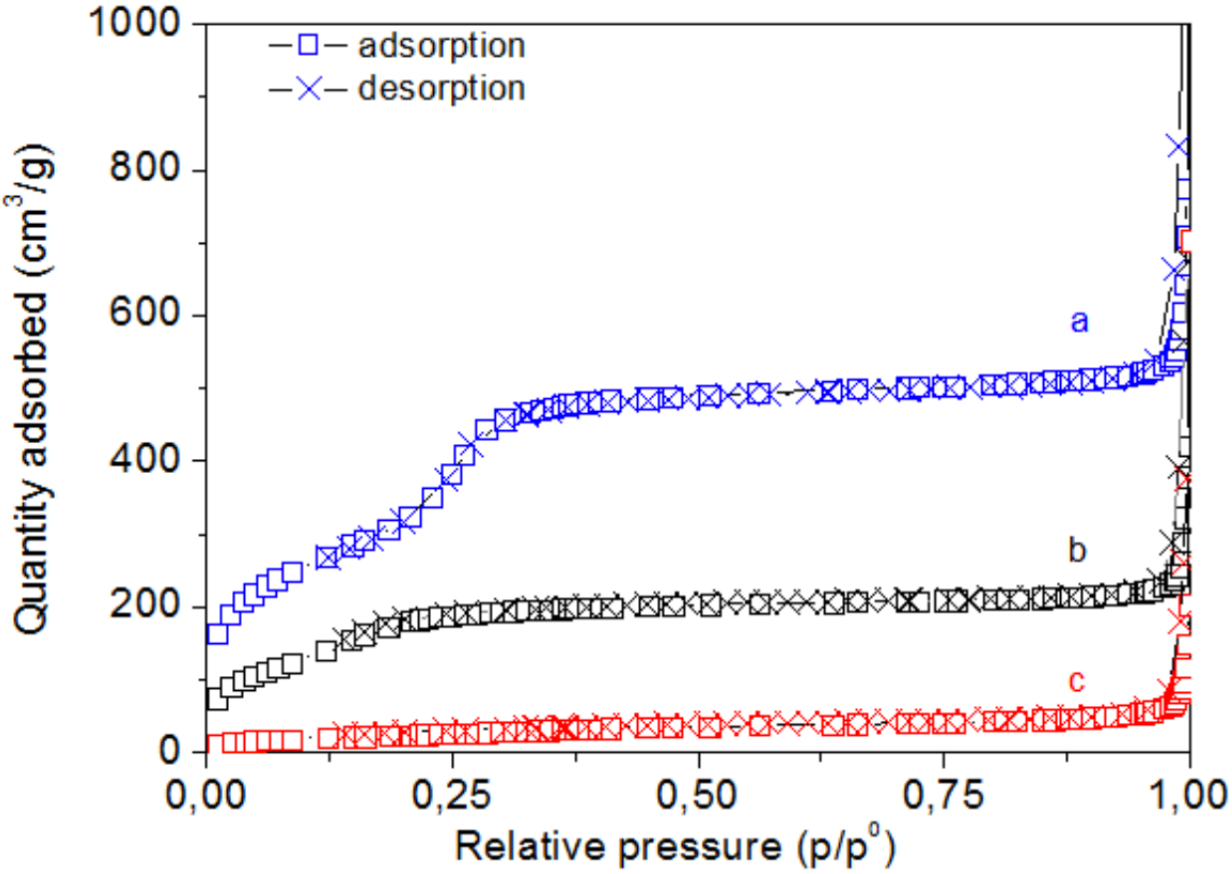
adsorption
desorption
Quantity adsorbed (cm3/g)
1000
800
600
400
200
0
a
b
c
0,00
0,25
0,50
0,75
1,00
Relative pressure (p/p0)

Fig. 4

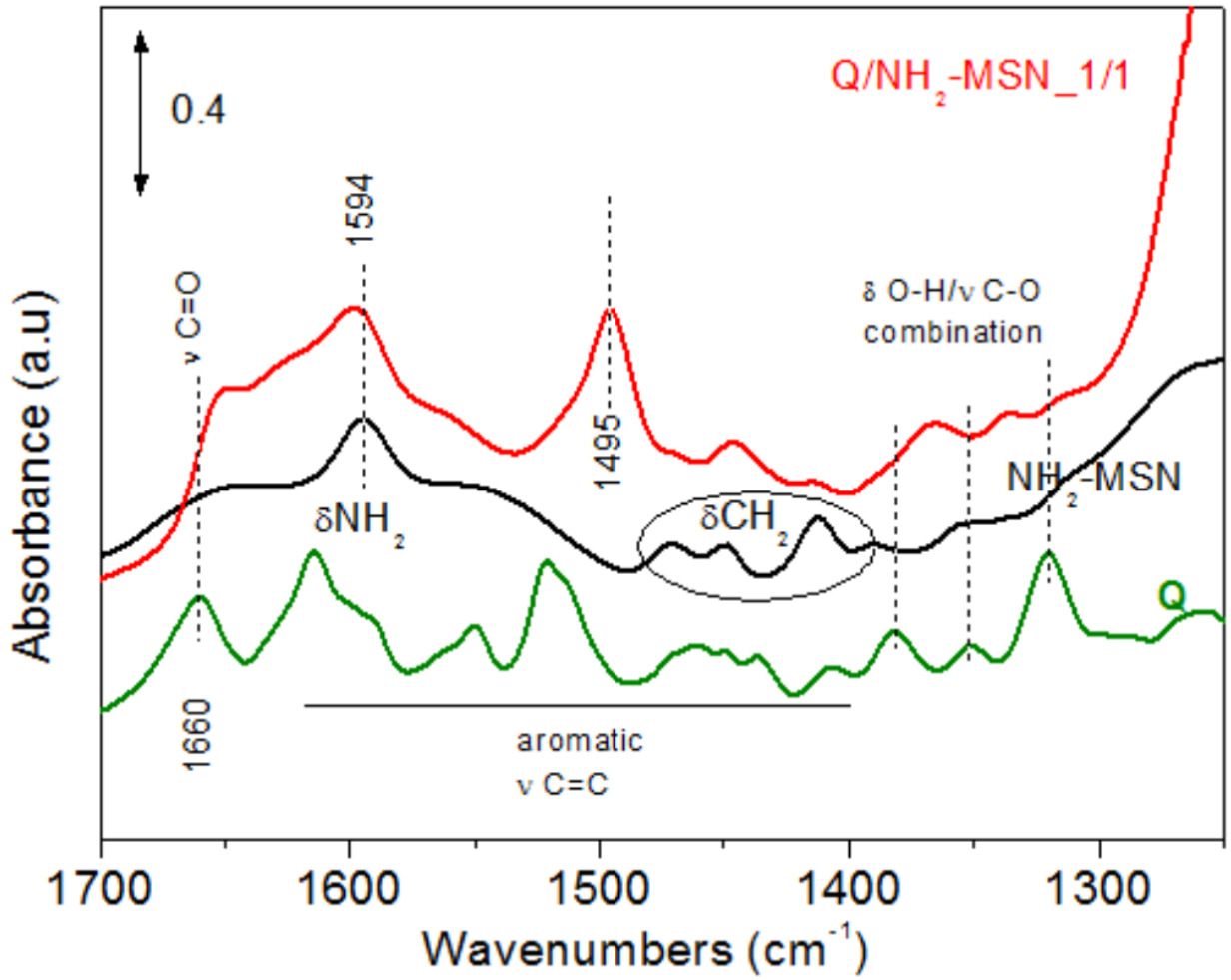
Q/NH2-MSN_1/1
0.4
1594
ν C=O
1495
δ O-H/ν C-O
combination
NH2-MSN
δNH2
δCH2
Q
1660
aromatic
ν C=C
Absorbance (a.u)
1700
1600
1500
1400
1300
Wavenumbers (cm-1)

Fig. 5 (top)

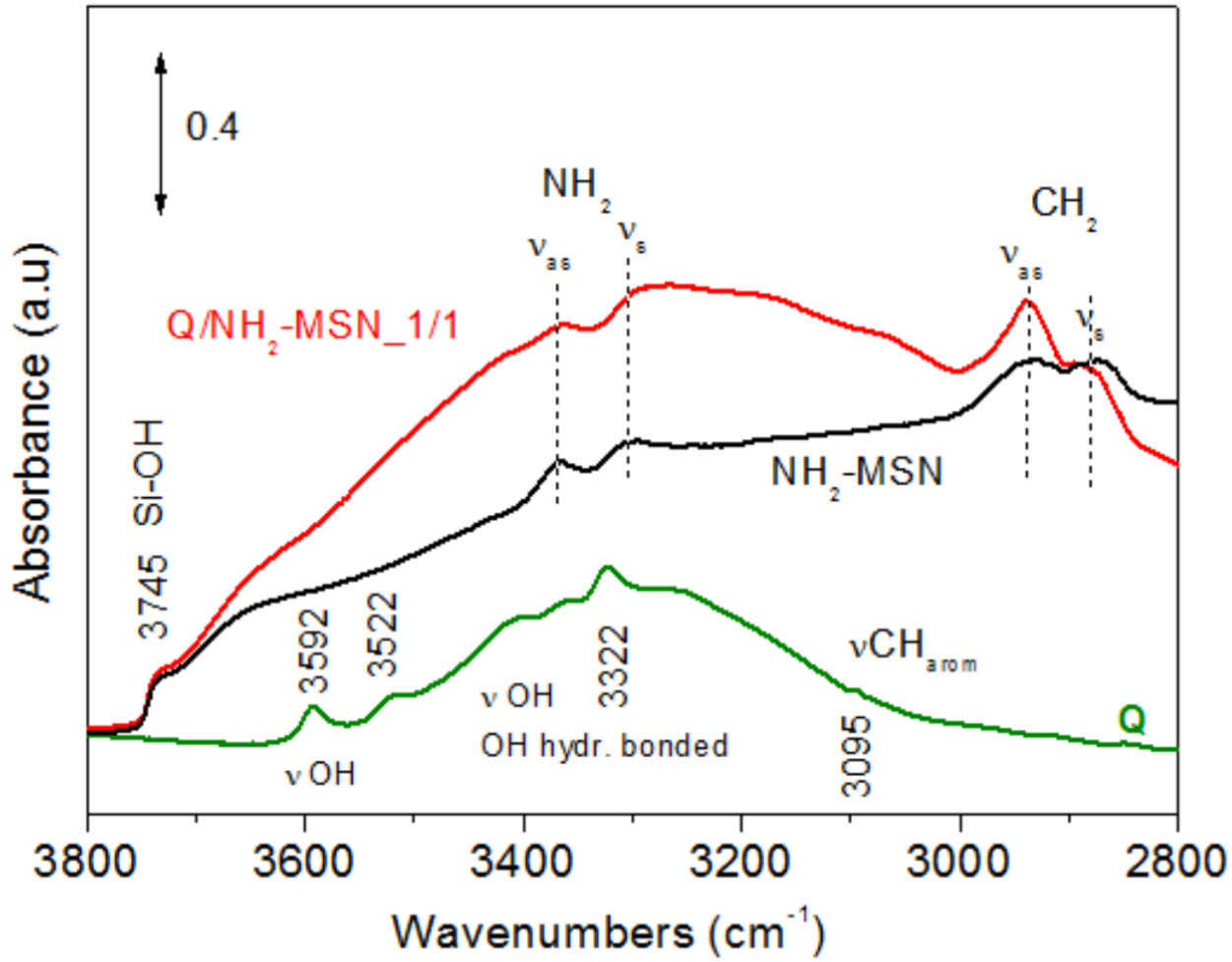
0.4
NH2
νas
νs
CH2
νas
νs
Q/NH2-MSN_1/1
NH2-MSN
Si-OH
3745
3592
3522
ν OH
ν OH
OH hydr. bonded
3322
νCHarom
3095
Q
Absorbance (a.u)
3800
3600
3400
3200
3000
2800
Wavenumbers (cm-1)

Fig. 5 (bottom)

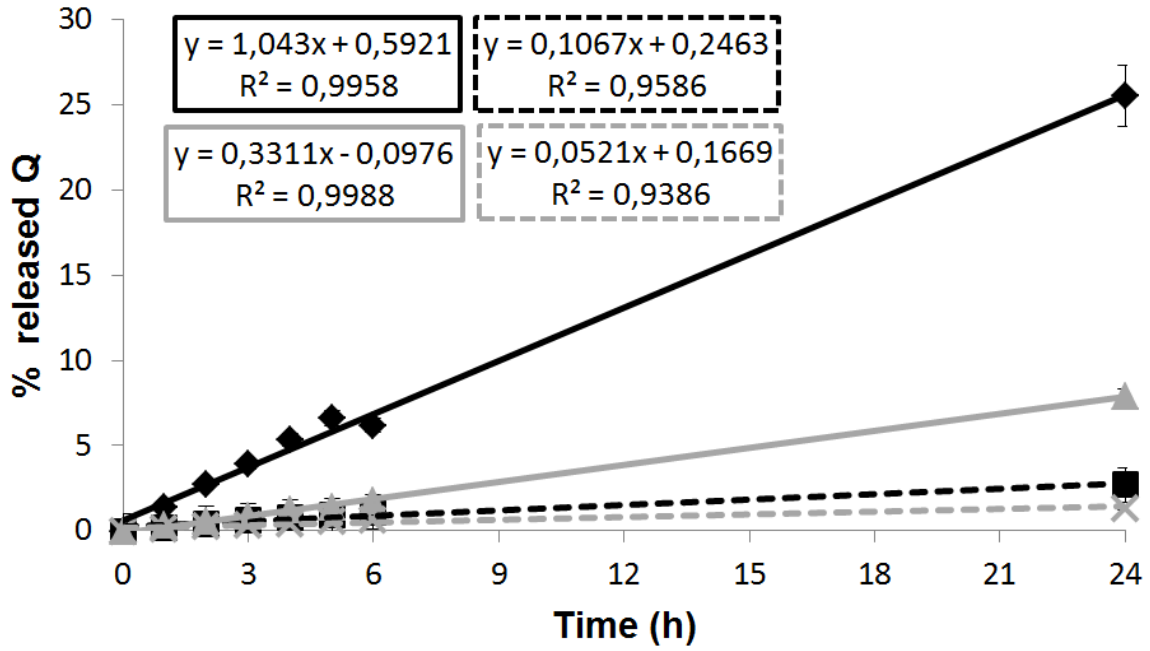
y = 1,043x + 0,5921
R² = 0,9958
y = 0,1067x + 0,2463
R² = 0,9586
y = 0,3311x - 0,0976
R² = 0,9988
y = 0,0521x + 0,1669
R² = 0,9386
% released Q
Time (h)
0
5
10
15
20
25
30
0
3
6
9
12
15
18
21
24

Fig. 6

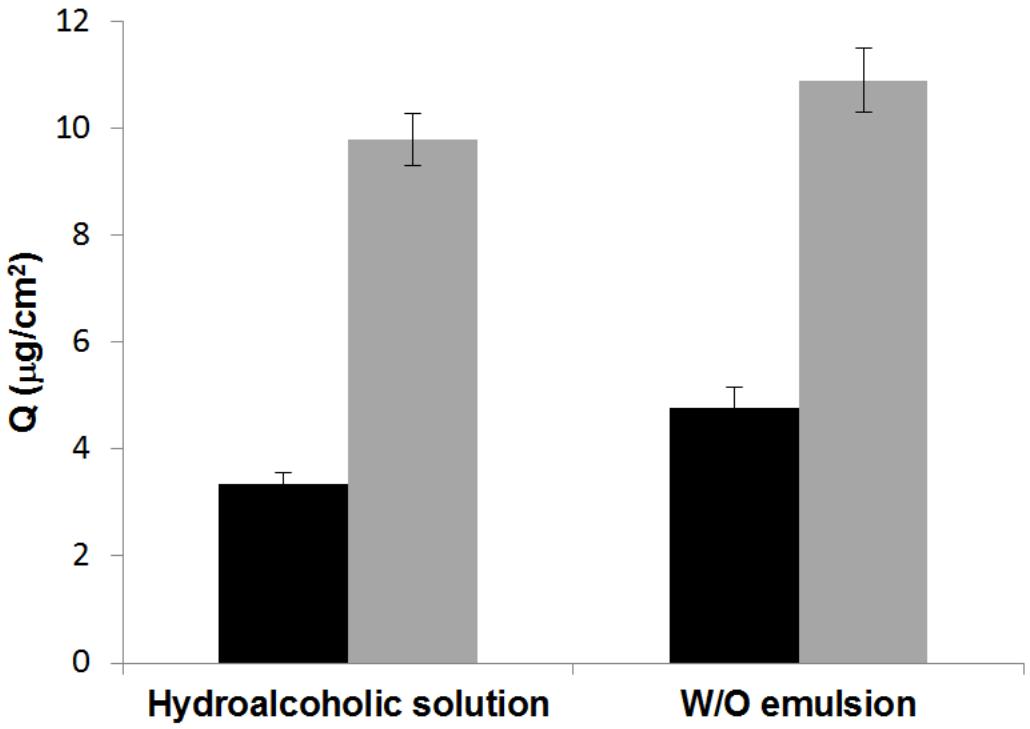

Fig. 7

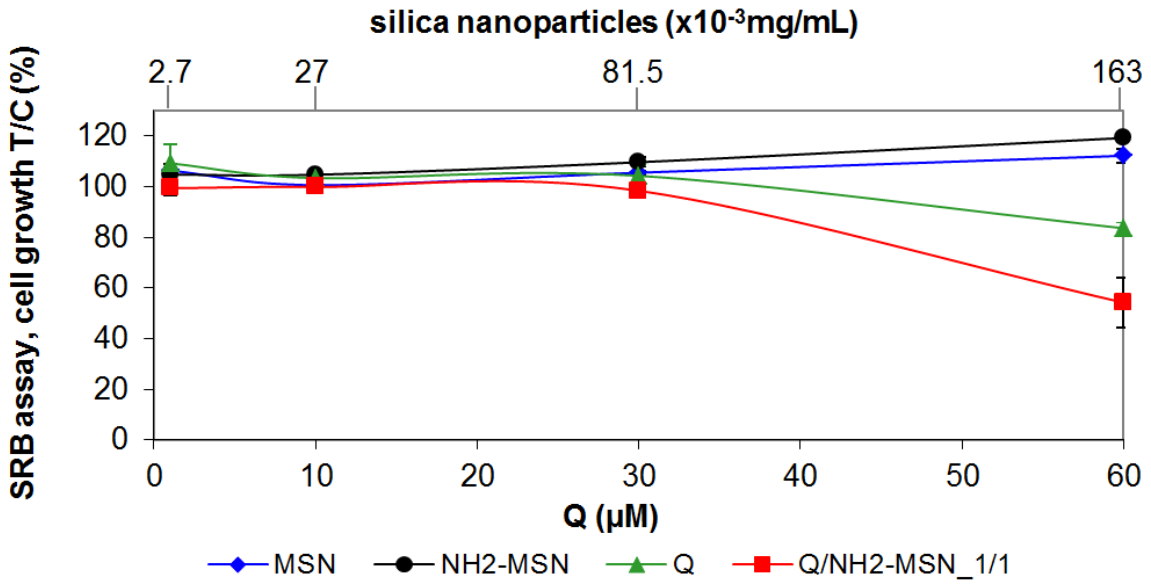
silica nanoparticles (x10-3mg/mL)
2.7
27
81.5
163
SRB assay, cell growth T/C (%)
120
100
80
60
40
20
0
0
10
20
30
40
50
60
Q (μM)
MSN
NH2-MSN
Q
Q/NH2-MSN_1/1

Fig. 8

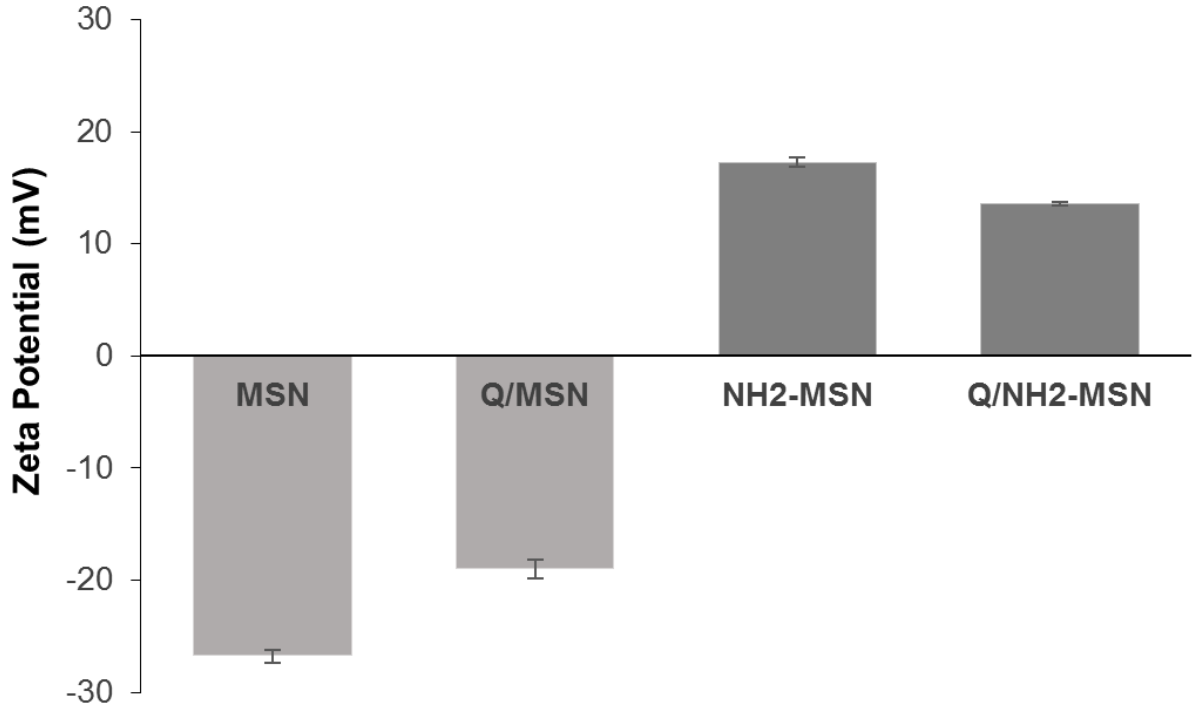

Fig. S1